Optical and Quantum Electronics (2005) 37:755–787
DOI 10.1007/s11082-005-8609-0

The fractional Fourier transform in the analysis and synthesis of fiber Bragg gratings

ENRICO MAZZETTO[1], CARLO G. SOMEDA[1], JUAN A. ACEBRÓN[2] AND RENATO SPIGLER[3,*]
[1]*Dipartimento di Ingegneria dell'Informazione, Università di Padova, Via Gradenigo 6/B-35131 Padova, Italy, E-mail: someda@dei.unipd.it*
[2]*Departamento de Automática, Escuela Politécnica, Universidad de Alcalá de Henares, Crta. Madrid-Barcelona, Km. 31.600 28871 Alcalá de Henares, Madrid, Spain, E-mail: juan.acebron@uah.es*
[3]*Dipartimento di Matematica, Università di "Roma Tre", Largo S. L. Murialdo, 1 – 00146 Roma, Italy (*author for correspondence: E-mail: spigler@mat.uniroma3.it)*

Received 1 February 2005; accepted 10 June 2005

Abstract. An approach based on the fractional Fourier transform is proposed for both analysis and synthesis of fiber Bragg gratings. The method is shown to be simple and accurate. A comparison is made with the results of the numerical integration of the full Riccati equation, which are valid for arbitrary reflectivities. The method being very efficient, processing times can be short enough for a real-time control of the writing process, during grating manufacturing. The effects of profile random irregularities on FBG performance are studied, and several examples, useful for design purposes, are given.

Key words: fiber Bragg gratings, fractional Fourier transform

1. Introduction

The present popularity of fiber Bragg gratings (FBGs) is so widely documented in the literature that it does not need any additional comment. Interest in FBG filters is expected to remain high in the future too, since exploiting all the potential bandwidth of optical fibers remains a fundamental issue. Another growing source of interest in FBGs comes from their use as transducers in fiber sensing systems. Consequently, the ranges in specifications, performances and prices of FBGs are very wide, and there is no reason why we should expect them to shrink.

The basic mechanisms on which FBGs rely are now part of any educational program on optical communications. Several modeling and design tools for FBGs are easily available (e.g., see (Keren *et al.* 2003) and the list of references therein). A widely used approach for analyzing FBGs is based on the transfer matrix method (Ouellette *et al.* 1994). Its implementation may require, at best of our knowledge, such short times to represent a real advantage. Another, less employed, numerical approach was proposed, based on Rouard's method (Weller-Brophy and Hall 1985, 1987,

1988; Baghdasaryan *et al.* 2005). This is a recursive technique, used in thin film coating design, similar to the transfer matrix method. More precisely, it consists in dividing the grating into a number of sections (as it is done in the transfer matrix method) and then subdivide into further thin layers in order to model the refractive index accurately. It was shown (Weller-Brophy and Hall 1987) that Rouard's method yields results in excellent agreement with those obtained by the coupled-mode theory to within 1% differences in the computed reflectivities. While the method can be used to analyze complex-shaped grating profiles, it is very time consuming and restricted by computational errors when calculating the spectral response of a large number of thin films (Kashyap 1999). The most clear-cut method to analyze Bragg gratings is perhaps through direct numerical integration of the coupled-mode equations. This is not the fastest method but it is well suited to model fairly complex grating profiles, providing highly accurate results at the same time. Indeed, the classical fourth-order Runge-Kutta algorithm seems to work well to this purpose (Erdogan 1997).

The common drawback remains, however, to miss to provide analytical results. Therefore, we believe that the growing interest in this topic makes it worthy to look for alternative approaches. Merits that new techniques should have, in order to be useful, consist of contributing to the physical understanding, or yielding faster numerical design tools, or lending themselves to a two-way use, i.e. to going from the refractive index profile to the filter transfer function *and* vice-versa.

Among the numerous approaches to FBGs which are already in use, some exploit the approximate Fourier transform relation between the filter spectral response (reflection coefficient) and the grating coupling function (index profile). However, this amounts to a first-order Born approximation, i.e., to neglecting the nonlinear term in the Riccati equation which describes more rigorously the local reflection coefficient. Therefore, these methods are expected to be satisfactory only for low-reflectivity filters. An alternative approach is represented by several techniques that are based on electromagnetic inverse scattering. Among them, the so-called layer-peeling, or dynamic deconvolution algorithms, seem to be very efficient. The latter method was introduced by Feced *et al.* (1999), and later applied, e.g., in (Skaar *et al.* 2001, Wang and Erdogan 2001). Accuracy is a plus of this method, but the price to pay is that it is substantially more complex, and its numerical implementation is time consuming.

With these motivations, we focused on an approach based on the so-called *fractional Fourier transform* (f FT). Our attention was drawn on this mathematical technique by its formal similarity to Fresnel diffraction integrals, which, in turn, had already been exploited in modeling and designing FBGs (Bonino *et al.* 1997). The similarity between spectral response of a linearly chirped FBG and Fresnel diffraction was also

observed and exploited by other authors (see (Azana and Muriel 2001), e.g., for an overview).

We believe that the results presented in this paper show that this new approach has at least some of the previously listed merits, and possibly all of them. Preliminary explorations of this subject were made, within our group, a few years ago (Braghetto 1998; Galli 1999; Schiavone 2000). However, all these remained unpublished. To the best of our knowledge, application of the f FT to FBGs is discussed here for the first time in the open literature.

Another relevant background item is that many gratings are characterized by 'linearly chirped' index profiles. Probably, these represent the most important class of all FBGs. If the chirp term is embodied in the kernel of the aforementioned Fourier transform, then the resulting relationship can be interpreted as the f FT of a simpler profile. The case of 'no chirp' can be recovered as a special case, and the fFT reduces, correspondingly, to the ordinary Fourier transform. An ensuing advantage is that one can tabulate, analytically, results that correspond to a number of important cases. On other occasions, one just evaluates numerically such an explicit integral formula. We will show here that this procedure can be accomplished in a very short time, at least 3 orders of magnitude faster than the numerical solution of the Riccati equation, for comparable accuracy. In addition, the same approach provides, with comparable speed, the inverse relationship, i.e. the index profile from the spectral behavior of the reflection coefficient. Such a method, being so fast, appears to be suitable for real-time control of the grating writing, during the FBGs manufacturing process.

The paper is organized as follows. In Section 2, we recall the fundamentals of the f FT. Those readers who are familiar with this chapter of mathematics can skip this part. In Section 3, we show in detail, with a general theory and a set of examples, how the f FT can be exploited in the *analysis* of an FBG with a given index profile. Section 4 is devoted to a problem analysis in terms of spline functions, which, in our opinion, plays a crucial role in linking the idea of f FT to practical applications. The method described in this paper can be generalized to include a cascade of several grating segments, each having a different chirp coefficient, thus widening its range of applicability. Section 6 deals with the *synthesis* problem, i.e., how to use the f FT to reconstruct the index distribution from the transfer function of an FBG. It encompasses a set of four examples. In Section 5, it is shown that our approach is capable of handling random errors, without claiming its superiority with respect to other existing methods, under this point of view. We note that using splines, both direct and inverse fFT can be evaluated for general profiles, that are given only through a discrete set of values. Therefore, both analysis and synthesis of FBGs can be accomplished in this way. Finally, in Section 7 we draw our conclusions, outline the advantages of this approach, and discuss its limitations.

2. Background

The fractional Fourier transform (f FT) was first introduced by Namias (1980) to solve certain problems in Quantum Mechanics, and later developed rigorously by McBryde and Kerr (1987). Numerous applications have been proposed since then; see, e.g., the recent book (Ozaktas *et al.* 2001). There exist several versions of the f FT; we adopt the so-called 'chirped f FT' (sometimes denoted as CFRT). The fractional Fourier transform of (real) order a of the function $s(t)$ is then defined as

$$S_a(f) \equiv \mathcal{F}^{\alpha}[s(t)] = K_a e^{j\pi B_a f^2} \int_{-\infty}^{+\infty} s(t) e^{j\pi B_a t^2} e^{-j2\pi C_a f t} \mathrm{d}t \tag{1}$$

where

$$C_a = \csc\left(\frac{\pi}{2}a\right), \qquad B_a = \cot\left(\frac{\pi}{2}a\right),$$

$$K_a = \sqrt{1 - jB_a} = \left|\csc\left(\frac{\pi}{2}a\right)\right|^{1/2} e^{j\frac{\pi}{4}\left(a - \mathrm{sign}(\sin(\frac{\pi}{2}a))\right)} \tag{2}$$

for suitable functions $s(t)$. It is immediately recognized that $S_a(f)$ reduces to the ordinary Fourier transform (FT) when $a = 1$, being $C_a = K_a = 1$, $B_a = 0$ in this case. If we set (formally) $a = -1$, the inverse FT is recovered. Due to a certain similarity between the f FT and the FT, one can expect that many properties of the latter have a counterpart for the former. Indeed, this is the case, and a number of such properties have been catalogued in (Namias 1980; McBryde and Kerr 1987; Erseghe 1996; Ozaktas *et al.* 2001). The additional degree of freedom enjoyed by the f FT provided by the extra parameter a can also be exploited in some problems. Among other things, it was observed that the f FT could be used to solve diffraction problems, cf. (Pellat-Finet 1994; Braghetto 1998; Ozaktas *et al.* 2001).

The similarity between the formula for the diffracted field in the Fresnel region, and the reflectivity of fiber Bragg gratings (FBGs), pointed out, e.g., in (Bonino *et al.* 1997), then suggests to use the f FT to evaluate such reflectivity, given the refractive index profile. This point of view was first tested in (Braghetto 1998). Subsequently, preliminary numerical experiments (Galli 1999) showed that this approach could indeed entail shorter CPU times, compared to the conventional approaches. Finally, the possibility of using the f FT and its inverse also for the synthesis of FBGs (i.e., from the reflectivity to the index profile) was pointed out in (Schiavone 2000). All these tasks were pursued further in (Mazzetto 2003). However, as we said before, these preliminary results were not published.

3. Basic analysis

Let us start from the well established representation of the complex-valued reflection coefficient of an FBG, r, in terms of the FBG refractive index profile, expressed as a function of the longitudinal coordinate, z. This expression for r is, as well known, a fallout of the 'coupled mode approximation' (Yariv 1973), and therefore is restricted to low per-unit-length reflectivities. Assuming low local reflectivity allows us to neglect the quadratic term in the Riccati differential equation which is satisfied, rigorously, by r (Kogelnik 1976; Song and Shin 1985; Mazzetto 2003). Hence, we obtain

$$r(\xi) \equiv r\left(-\frac{\pi}{\Lambda}\frac{\Delta\lambda}{\lambda}\right) = -\int_{-\infty}^{+\infty} \kappa\, \gamma(z)\, e^{j\left(-\frac{2\pi}{\Lambda}\frac{\Delta\lambda}{\lambda}z + \frac{2\pi}{\Lambda}\frac{C}{\Lambda}z^2\right)}\, \mathrm{d}z, \tag{3}$$

where λ is the optical wavelength (in free space), Λ is the grating period, $\lambda_B = 2n_{\mathrm{eff}}\Lambda$ the so-called Bragg (central) wavelength, n_{eff} being the effective mode index, $\Delta\lambda = \lambda - \lambda_B$, κ is the coupling coefficient of the two counterpropagating modes, following Yariv's notation (and can be taken to be constant vs. z), and $\gamma(z)$ represents the tapering function of the grating. The index of refraction is assumed to be of the form

$$n(z) = n_0 + \Delta n(z), \quad \Delta n(z) = A\gamma(z)\cos\left(\frac{2\pi}{\Lambda}z + \phi(z)\right), \tag{4}$$

where $A = \kappa\lambda_B/\pi$ is the index step, and the phase term, $\phi(z)$, is a 'chirp',

$$\phi(z) = -\frac{2\pi}{\Lambda^2}Cz^2, \tag{5}$$

with the 'chirp coefficient' $C = -\frac{1}{2}\frac{\Delta\Lambda}{L}$. The FBG is assumed to lie on the interval $[-L/2, L/2]$ of the z axis.

To express r as a fractional Fourier transform, let us use (1)–(2). We get:

$$r(\xi) = -\kappa\frac{\Lambda}{\sqrt{2C'}}\sqrt{\cos\alpha}\, e^{-j\frac{\pi}{4}}\, e^{-j\frac{\alpha}{2}}\, e^{-j\pi\cot\alpha\,(\xi/A_2)^2}\, \mathcal{F}^{\alpha}[\gamma(A_1 z)]\left(\frac{\xi}{A_2}\right), \tag{6}$$

where $C' = -C, \alpha = \pi a/2$, and

$$A_1 = \frac{\Lambda}{\sqrt{2C'|\tan\alpha|}}, \quad A_2 = \frac{\pi\sqrt{2C'}}{\Lambda\sqrt{|\sin\alpha|\cos\alpha}}. \tag{7}$$

To be valid, Equations (6), (7) require that $-\pi/2 < \alpha < 0$ (i.e., $-1 < a < 0$). This does not imply any loss of generality.

From Equation (3) or Equation (6), one proceeds, usually, to evaluate the *reflectivity*, i.e. the reflected fraction of the guided power, $R = |r|^2$. The

numerical evaluation of the right-hand side of (3) is beset by the chirp term, which makes the integral a very rapidly oscillatory one. As a result, it may be very time-consuming. On the other hand, as we will see soon, for a large number of profiles $\gamma(z)$ of practical interest, the f FTs are easy to compute analytically. Having their general expressions at hand, makes it fast and efficient to evaluate $r(\xi)$ when the FBG parameters are specified. In the next Section we will see how these advantages can be extended also to profiles that do not belong to classes whose f FTs are known.

Let us support our claim with examples, characterized by various taper functions, $\gamma(z)$. Since the FBG is assumed to be located in $[-L/2, L/2]$, any profile will be of the form

$$\gamma(z) = g(z)\mathrm{rect}\left(\frac{z}{L}\right) \tag{8}$$

where $g(z)$ is defined on the entire z axis. Symbols have been defined at the beginning of this Section; let W be the width at half-maximum ($FWHM$). Unless otherwise stated in the captions, the numerical results presented in the figures refer to the following parameter values, chosen as typical of practical FBGs: $A = 3 \times 10^{-5}$, $C = -24 \times 10^{-10}$, $\lambda_B = 1.552\,\mu$m, $L = 7$ cm and $n_{\mathrm{eff}} = 1.4486$, cf. (Erdogan 1997; McCall 2000; Mazzetto 2003).

Example 1. Let us start with the simplest profile, namely that with *constant* index step, i.e.

$$g(z) = 1, \qquad \gamma(z) = \mathrm{rect}\left(\frac{z}{L}\right). \tag{9}$$

We must evaluate the f FT of $\gamma(A_1 z) \equiv \mathrm{rect}(z/2D')$, where we set $D' = D/A_1$, $D = L/2$. Recalling (7) and (2), we get

$$\mathcal{F}^{\alpha}\left[\mathrm{rect}\left(\frac{z}{2D'}\right)\right](x) = (1+j)\frac{K_a}{2\sqrt{2B_a}}\, e^{-j\pi x^2/B_a}\left[\mathrm{erf}(x_+) - \mathrm{erf}(x_-)\right], \tag{10}$$

where $\mathrm{erf}(x)$ denotes the error function (Abramowitz and Stegun 1970), and

$$x_{\pm} = (1-j)\sqrt{\frac{\pi}{2}}\left(\pm\sqrt{B_a}D' - \frac{C_a}{\sqrt{B_a}}x\right). \tag{11}$$

A little algebra yields

$$r(\xi) = -\kappa\,\frac{\Lambda}{\sqrt{2C'}}\sqrt{\cos\alpha}\, e^{-j\pi/4} e^{-j\alpha/2} e^{-j\pi(\cot\alpha)(\xi/A_2)^2}\mathcal{F}^{\alpha}\left[\mathrm{rect}\left(\frac{z}{2D'}\right)\right]\left(\frac{\xi}{A_2}\right). \tag{12}$$

In Fig. 1, the reflectivity computed via the fFT is compared with the result obtained by numerical integration of (3). The fFT approach requires a significantly shorter CPU time. Furthermore, it is more accurate in the low-reflectivity tails, where the rapidly oscillating term in (3) introduces significant errors, cf. (Mazzetto 2003).

In order to make the comparison in terms of accuracy as significant as possible, we also solved numerically the following Riccati equation, for which (3) represents, as we said before, an approximate solution, where the nonlinear term is neglected:

$$\frac{\mathrm{d}r}{\mathrm{d}z} = -2j\xi\, r + \kappa\gamma(z)e^{-j\phi(z)} - \kappa\gamma(z)e^{j\phi(z)}r^2, \tag{13}$$

where the local reflection coefficient is $r(z,\xi) = E_2(z,\xi)/E_1(z,\xi)$, where E_1, and E_2 are the complex amplitudes of the modes propagating along $+z$ and $-z$, respectively. In Fig. 2, the reflectivity computed from (13)

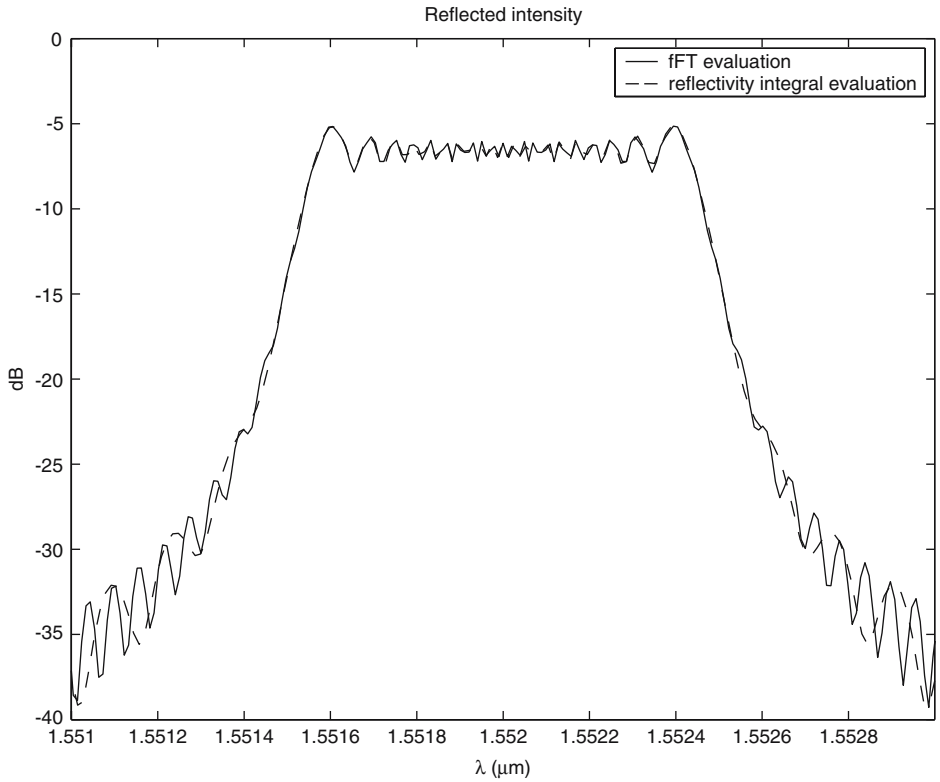

Fig. 1. Comparison between reflectivity evaluated by the fractional Fourier transform with $\alpha = -\pi/4$, and by the reflection integral; $L = 7$ cm.

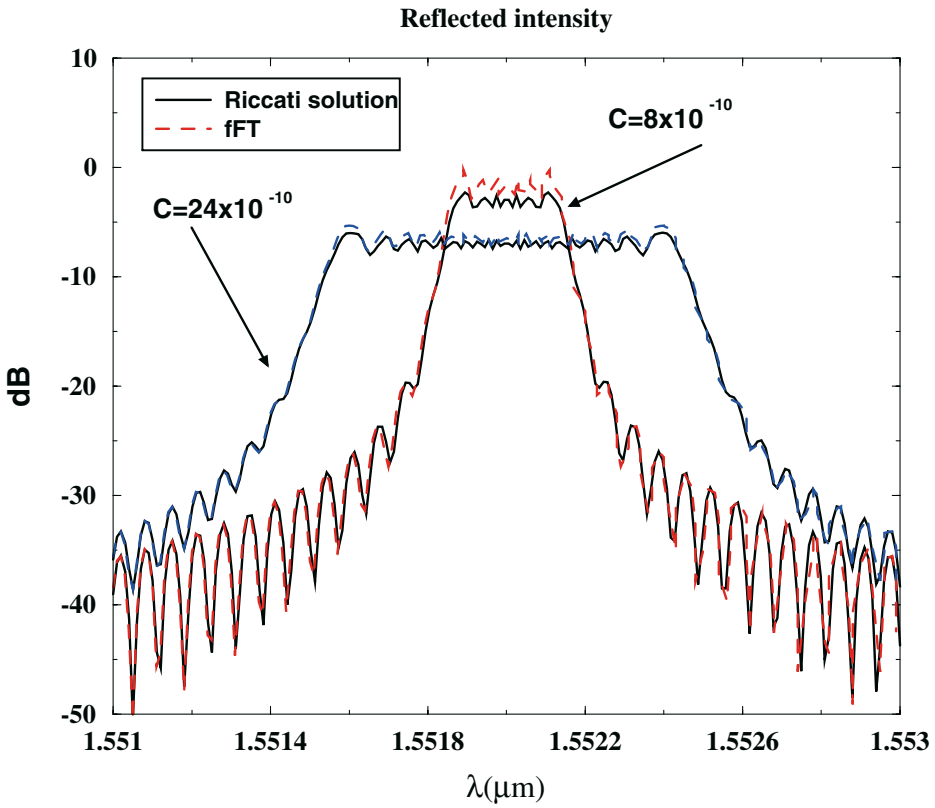

Fig. 2. Comparison between reflectivity evaluated by the fractional Fourier transform and numerical solution of the Riccati equation. Parameters are as in Fig. 1.

by Runge-Kutta methods is compared with that evaluated by the fFT. The agreement is excellent, despite the fact that the second method was expected to work well only under the condition of low reflectivity (i.e. under the Born approximation). The only significant difference between the two plots is that the fFT tends, systematically, to slightly over-estimate the reflectivity peak value in the stop-band. However, the shape of the spectral profile is preserved very accurately. Notice that the fourth-order Runge-Kutta algorithm has been implemented with a sufficiently small step size to make the numerical error negligible. The required CPU time (on a standard Pentium IV PC) was then 19.90 s, while the numerical evaluation of the fFT required only 0.01 s. The speed-up factor achieved amounts therefore to about 2×10^3. Two values of the chirp coefficient C have been used in Fig. 2, to test in more detail the behavior of the fFT.

Figures 3 and 4 show reflectivity profiles calculated as fFTs, that correspond to different values of the index step, A. The dependence of r on

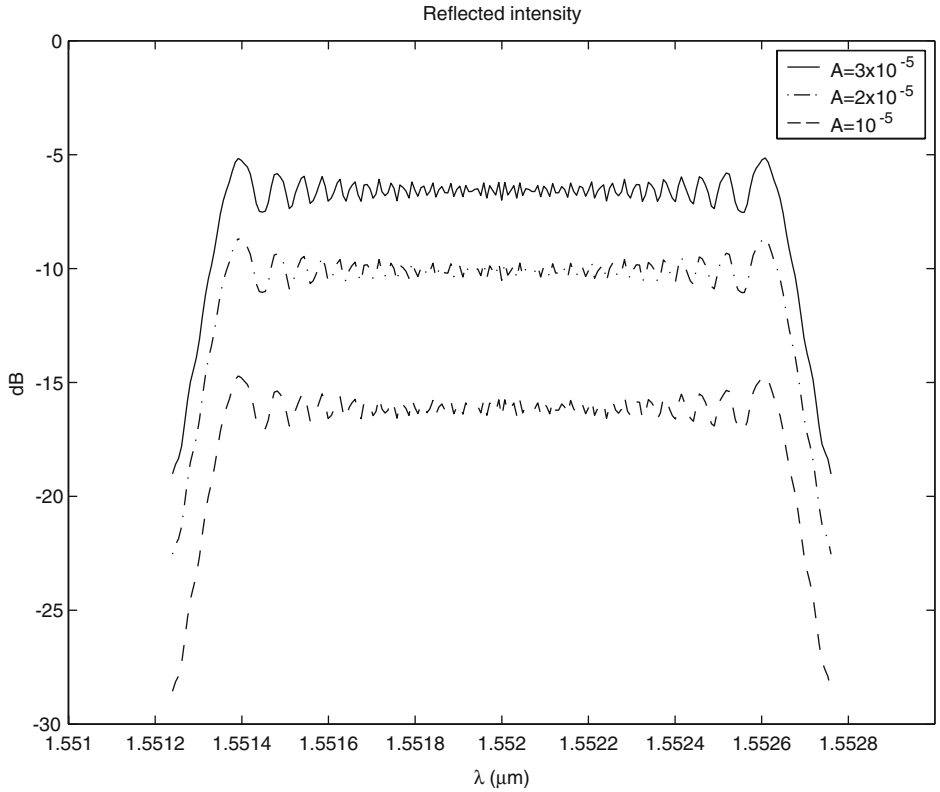

Fig. 3. Examples of fFT reflectivity for gratings with a constant index step, A, for several values of A; $\alpha = -\pi/4$, $L = 10\,\text{cm}$.

the FBG length, L, is illustrated by comparison between figures: as is well known, shorter filters have narrower frequency bands.

To further test how dependable the fFT results are when the index step, henceforth the reflectivity, becomes large, let us compare, once more, results based on fFT and those based on numerical integration of the full Riccati equation, for growing values of A. Figure 5 reconfirms what we just said about Fig. 2. The qualitative agreement remains excellent even for reflectivities close to unity. The spectral shape is preserved very accurately, both at the edges of the stopband and in the low-reflectivity tails. There is a systematic tendency of the fFT to slightly over-estimate the reflectivity in the stop-band.

Example 2. Let us deal with the *gaussian* profile

$$g(z) = e^{-\pi c z^2}, \tag{14}$$

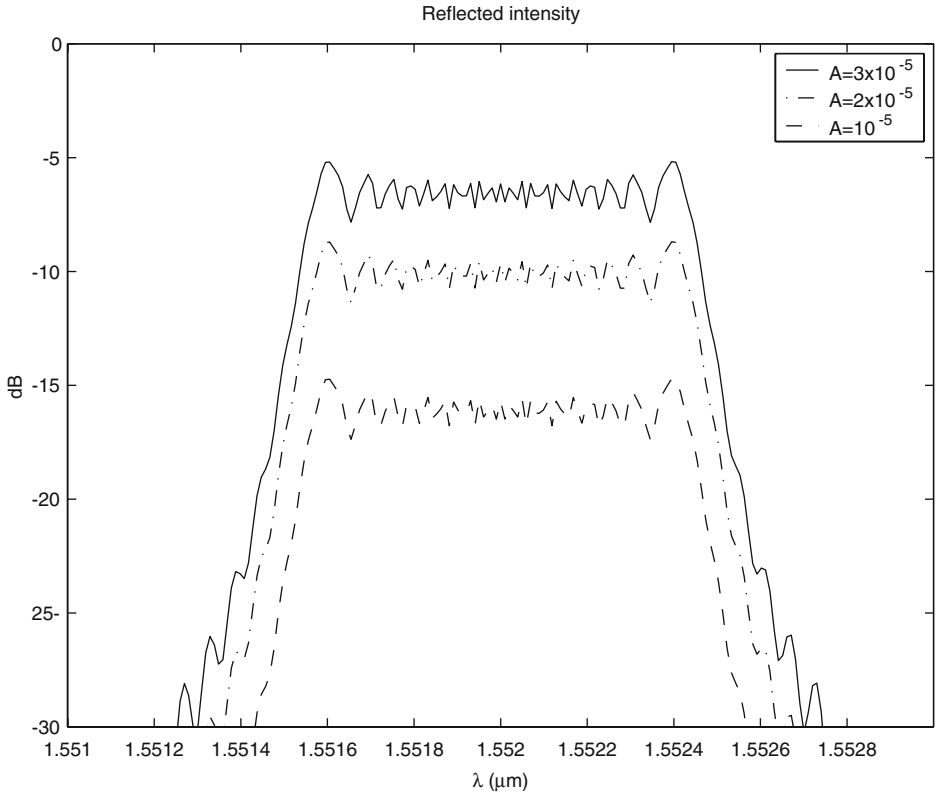

Fig. 4. As in the previous figure, with $L = 7\,\text{cm}$.

where $c = (4 \ln 2)/W^2$. We need to evaluate the f FT of

$$\gamma(z) = e^{-\pi c z^2} \operatorname{rect}\left(\frac{z}{L}\right) \tag{15}$$

taken on a suitable scale, i.e.

$$\gamma(A_1 z) = e^{-\pi c (A_1 z)^2} \operatorname{rect}\left(\frac{A_1 z}{L}\right) = e^{-\pi c' z^2} \operatorname{rect}\left(\frac{z}{2D'}\right), \tag{16}$$

and the fFT should be evaluated at the points ξ/A_2, being $D = L/2$, $D' = D/A_1$, $c' = cA_1^2$. We find

$$\mathcal{F}^{\alpha}\left[e^{-\pi c' z^2} \operatorname{rect}\left(\frac{z}{L}\right)\right](x) = (-1)^{1/4} \frac{K_a}{2\sqrt{B_a + jc'}} \times e^{j\pi\left(B_a - \frac{C_a^2}{B_a + jc'}\right)x^2} [\operatorname{erf}(x_+) - \operatorname{erf}(x_-)], \tag{17}$$

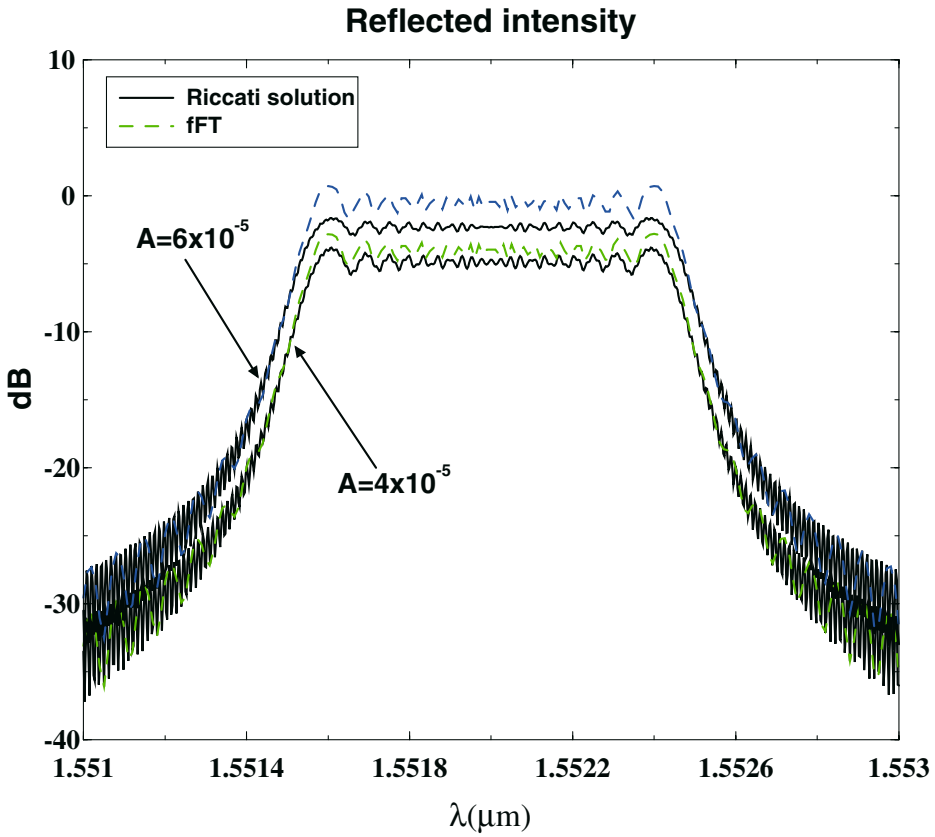

Fig. 5. Comparison between reflectivity obtained by Riccati equation and by the fractional Fourier transform for two values of the index step, A.

where

$$x_{\pm} = -(-1)^{3/4}\sqrt{\pi}\left(\frac{\pm(B_a + jc')D' - C_a x}{\sqrt{B_a + jc'}}\right). \tag{18}$$

After a little algebra, we get

$$r(\xi) = -\kappa \frac{\Lambda}{\sqrt{2C'}} \sqrt{\cos\alpha}\, e^{-j\pi/4} e^{-j\alpha/2} e^{-j\pi(\cot\alpha)(\xi/A_2)^2} \times \mathcal{F}^{\alpha}\left[e^{-\pi c' z^2} \operatorname{rect}\left(\frac{z}{2D'}\right)\right]\left(\frac{\xi}{A_2}\right). \tag{19}$$

Figure 6 shows the plots of the reflectivity, compared with the reflectivity of the other profiles. The parameter W does not affect the shape of the curve. In fact, this is clear from Equation (17), since the term jc' only affects the modulus of the profile appreciably.

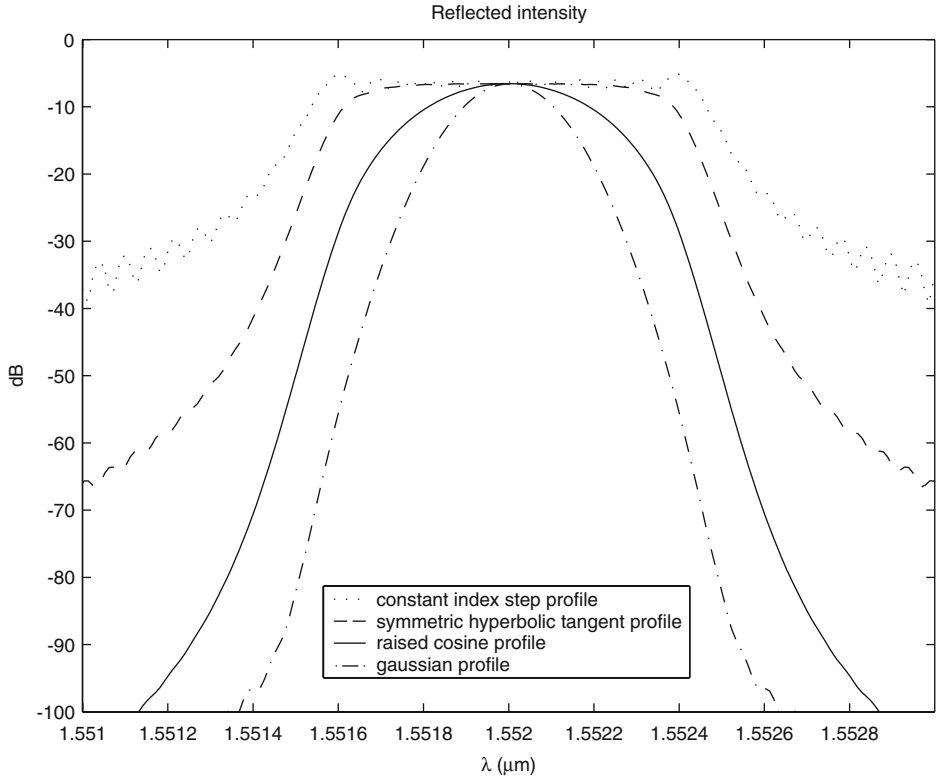

Fig. 6. Reflectivity for several index profiles; $\alpha = -\pi/4$, $L = 7$ cm.

Comparing this case to the uniform profile of Example 1, we see that several well-known results are reconfirmed: the gaussian profile yields higher selectivity, lower sidelobes, and steeper slopes.

Example 3. With the *raised cosine* profile with the usual truncation,

$$\gamma(A_1 z) = \frac{1}{2}\left[1 + \cos\left(\frac{\pi z}{W'}\right)\right] \operatorname{rect}\left(\frac{z}{2D'}\right), \tag{20}$$

where we set $W' = W/A_1$ and $D' = L/(2A_1)$, the f FT requires a little algebra, omitted here for the sake of brevity. The final result reads

$$\mathcal{F}^{\alpha}\left[\operatorname{cosr}(t) \operatorname{rect}\left(\frac{t}{2}D\right)\right](x) = \frac{A}{2} E_1 + ABCE_2 + AB^*CE_3, \tag{21}$$

where

$$
\begin{aligned}
&A = (1+j)\,\frac{K_a}{2\sqrt{2B_a}}\,e^{-j\pi x^2/B_a},\\
&B = \frac{1}{4}\exp\left(\frac{j\pi C_a}{DB_a}\,x\right), \quad C = \exp\left(-\frac{j\pi}{4D^2B_a}\right),\\
&E_1 = \operatorname{erf}\left(x_+^0\right) - \operatorname{erf}\left(x_-^0\right),\\
&E_2 = \operatorname{erf}\left(x_+^1\right) - \operatorname{erf}\left(x_-^1\right), \qquad E_3 = \operatorname{erf}\left(x_+^2\right) - \operatorname{erf}\left(x_-^2\right),\\
&x_\pm^0 = (1-j)\sqrt{\frac{\pi}{2}}\left(\pm\sqrt{B_a}D - \frac{C_a}{\sqrt{B_a}}\,x\right),\\
&x_\pm^1 = x_\pm^0 + \frac{\sqrt{\pi}(1-j)}{L\sqrt{2B_a}}, \qquad x_\pm^2 = x_\pm^0 - \frac{\sqrt{\pi}(1-j)}{L\sqrt{2B_a}}.
\end{aligned}
\tag{22}
$$

Figure 6 reconfirms a well-known nice feature of this profile: if we choose $W = L/2$, sidelobes in the reflectivity essentially disappear.

Example 4. Consider now the *symmetric hyperbolic tangent* profile,

$$\gamma_{\text{sym}}(z) = \tanh\left[T\left(1 - \frac{2|z|}{L}\right)\right]\operatorname{rect}\left(\frac{z}{L}\right), \tag{23}$$

along with the *asymmetric* profile

$$\gamma_{\text{asym}}(z) = \tanh\left(T\,\frac{|z - L/2|}{L}\right)\operatorname{rect}\left(\frac{z}{L}\right). \tag{24}$$

Here T is a parameter that characterizes the shape of the profile. To evaluate the transforms of the functions $\gamma_{\text{sym}}(A_1 z)$, $\gamma_{\text{asym}}(A_1 z)$, we have to resort to numerical calculations. In terms of efficiency, in this case the performance of the f FT technique is less favorable than in the previous examples.

Figure 7 shows the reflectivity corresponding to the symmetrical profile. A large sensitivity to the value of the parameter T is observed. For $T > 3$, the central part of the curve is very similar to that of a uniform profile (see Example 1), but is free of ripples. For smaller values of T, on the other hand, the profile looks closer to those of Examples 2 and 3, at the price of a smaller value (a few dB less) in the central peak. Figure 8 corresponds to the asymmetrical profile, whose practical application may be required only in special cases.

Example 5. (Super-gratings)**.** Consider now the case of a super-grating of constant sampling period d, made of $2n+1$ sections, each of length ℓ. It is described by the profile

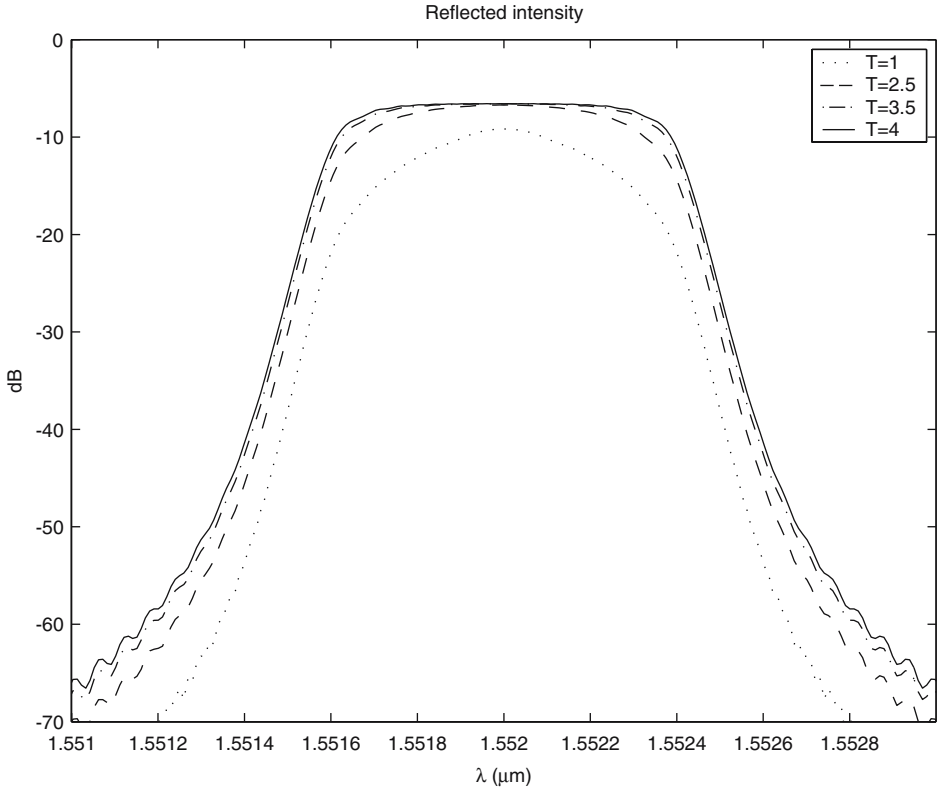

Fig. 7. Reflectivity for symmetric hyperbolic tangent profiles, for several values of the parameter T; $L = 7$ cm.

$$\gamma(A_1 z) = \sum_{i=-n}^{n} \text{rect}\left(\frac{A_1 z - id}{\ell}\right) = \sum_{i=-n}^{n} \text{rect}\left(\frac{z - id'}{\ell'}\right) \tag{25}$$

where we set $d' = d/A_1$, $\ell' = \ell/A_1$. In the numerical examples, we take $L = 10$ cm, $n = 2$, i.e. 5 sections, each $\ell = L/8$ in length, and $d = 3L/16$. Exploiting the linearity and shift properties of the f FT (Ozaktas *et al.* 2001), we evaluate

$$\begin{aligned}\mathcal{F}^{\alpha}[\gamma(A_1 z)]\left(\frac{\xi}{A_2}\right) &= \sum_{i=-n}^{n} \mathcal{F}^{\alpha}\left[\text{rect}\left(\frac{z - id'}{\ell'}\right)\right]\left(\frac{\xi}{A_2}\right) \\ &= \sum_{i=-n}^{n} R^{\alpha}\left(\left(\frac{\xi}{A_2}\right) - id'\cos\alpha\right) \times e^{-j2\pi i d' \frac{\xi}{A_2}\sin\alpha}\, e^{j\frac{\pi}{2} i^2 d'^2 \sin 2\alpha},\end{aligned} \tag{26}$$

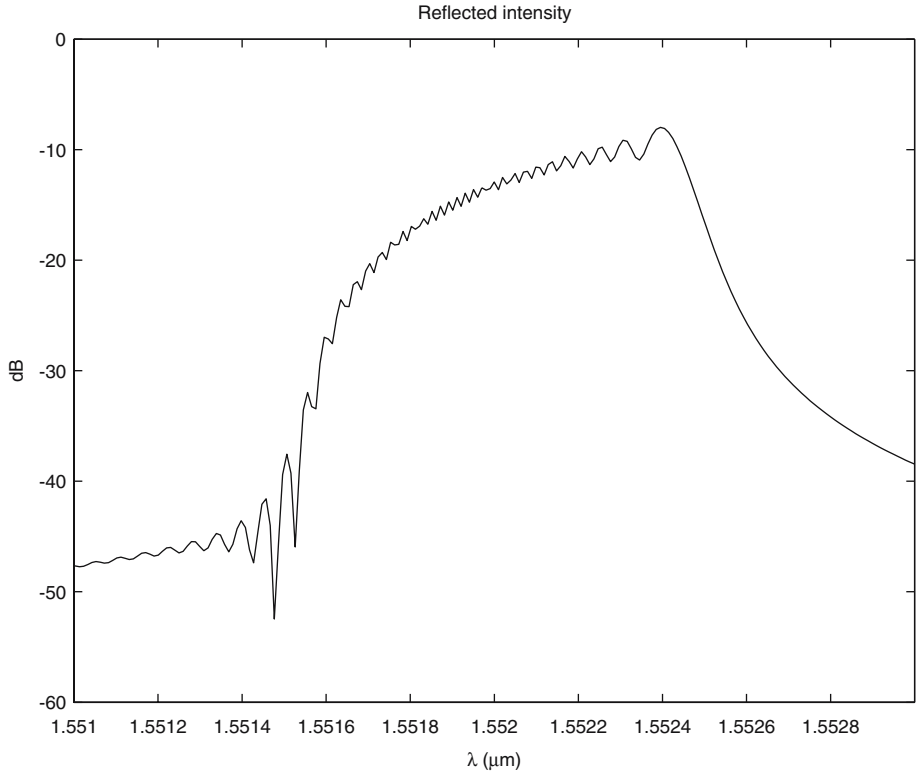

Fig. 8. Reflectivity for an asymmetrical hyperbolic tangent profile with $T=1$ and $L=7$ cm.

where R^{α} denotes the fFT of the function $\mathrm{rect}(\xi/\ell')$. The corresponding reflectivity is displayed in Fig. 9, which shows clearly that the super-grating, as expected, increases the bandwidth of every peak. On the contrary, if we reduce the value of the chirp, C, the peaks become narrower and sharper. The well-known formula $\Delta\lambda=\lambda_B^2/(2n_{\mathrm{eff}}d)=2n_{\mathrm{eff}}\Lambda^2/d=0.2$ nm, cf. (Ouellette *et al.* 1995), yielding the spectral range between peaks, is reconfirmed.

The super-grating case lends itself to validate the fFT approach by comparing it with the numerical solution of the Riccati Equation (13). In Fig. 9, we see that the two plots essentially coincide, except for slight discrepancies near the spike shoulders. Similarly to the case of the uniform grating, the speed-up factor in CPU time has been observed to be of order of 10^3 in this case too.

Examples of group delay. So far, our examples were focused on reflectivity, $|r(\xi)|^2$. The fFT, yielding a complex-valued reflection coefficient,

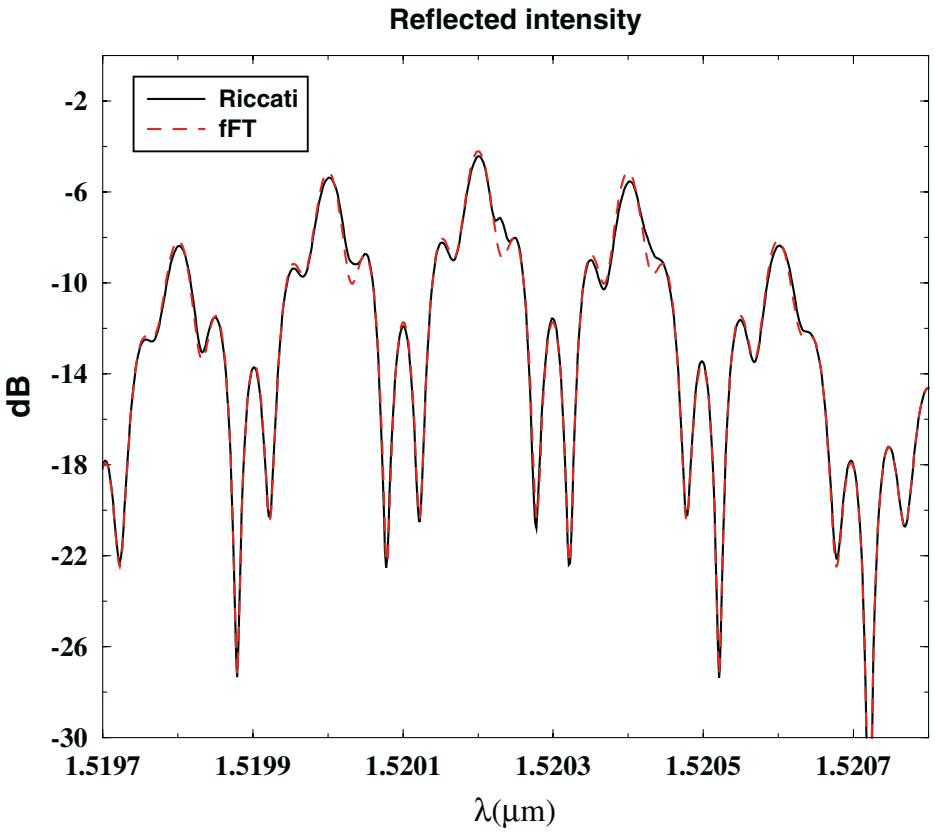

Fig. 9. Reflectivity for a super-grating with linearly varying pitch, with 5 sections, long $\ell = 1$ mm each, distant $d = 4$ mm. Solid line denotes the numerical solution of the Riccati equation, while the dashed line denotes the solution obtained using the fFT. Parameters are $\lambda_B = 1.5202$ μm, $C = -12 \times 10^{-10}$, $A = 8 \times 10^{-5}$.

$r(\xi) = |r(\xi)|\, e^{j\theta(\xi)}$, encompasses additional information concerning the *group delay*:

$$\tau = \frac{\mathrm{d}\theta}{\mathrm{d}\omega} = -\frac{\lambda^2}{2\pi c}\frac{\mathrm{d}\theta(\xi)}{\mathrm{d}\lambda}, \tag{27}$$

which is very useful for some applications of FBGs, first of all chromatic dispersion compensators. Figure 10 shows the group delay vs. wavelength, for various profiles that were introduced above. All these plots were obtained by means of the fFT, with numerical accuracy higher than in the previous examples, in order to guarantee that derivatives are accurate enough. The results agree very well with well-known ones, and lend themselves to simple physical explanations, in terms of how far the various

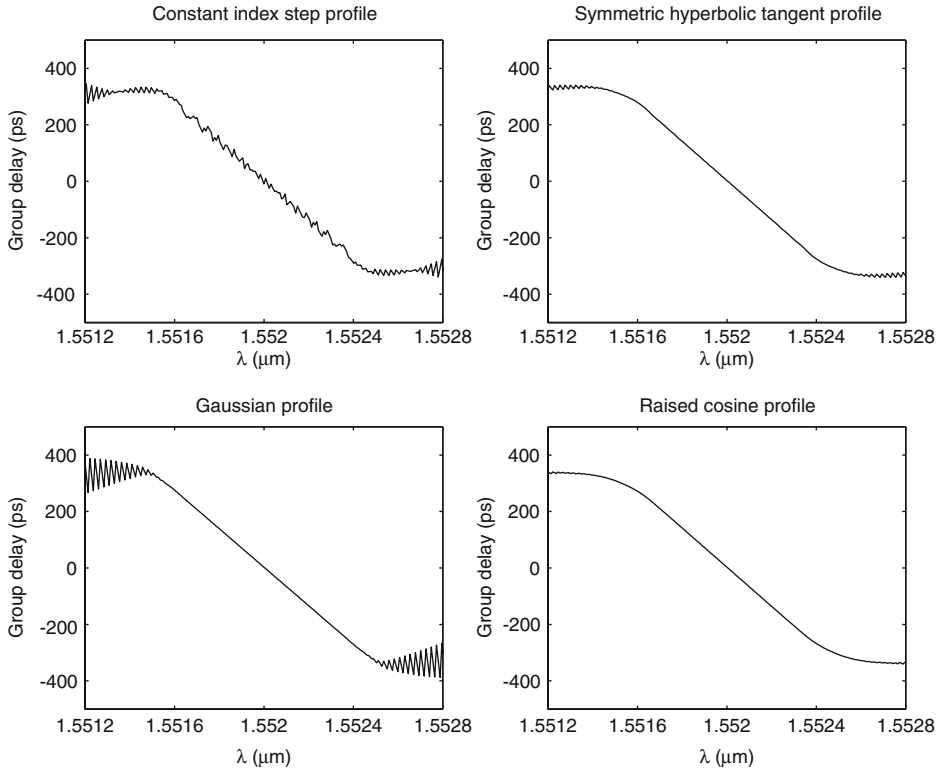

Fig. 10. Group delay for several index profiles; $\alpha = -\pi/4$, $L = 7\,\text{cm}$.

wavelengths penetrate into the grating, until they are strongly backward coupled by the appropriate grating pitch.

These results reconfirm that the taper profile affects the dispersion curve. The step profile, for instance, is not very satisfactory, because of ripples. The hyperbolic tangent profile appears to yield the most satisfactory results, in terms of high slope and low ripple.

To validate the new approach, group delays obtained via the fFT have been compared with those obtained by numerical integration of the Riccati Equation (13). Due to space limits, we will show only the case of a constant index step profile. An excellent agreement can be observed in Fig. 11, with a few, small discrepancies near the center of the spectral region of interest. Meanwhile, the speed-up factor achieved using the fFT is of order 10^3, as for the reflectivity.

To conclude this section, let us recall that one of the main criteria which drive the choice of an FBG profile is cost and complexity of fabrication. The adoption of the fFT does not provide any information under this

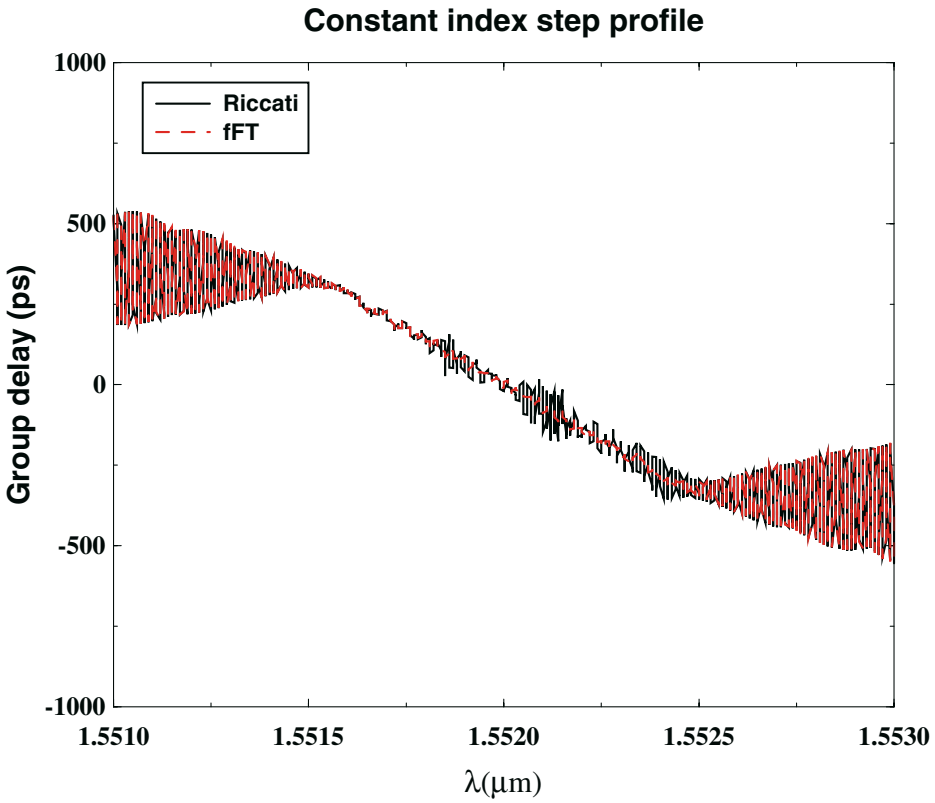

Fig. 11. Comparison between group delay evaluated by the fractional Fourier transform and numerical solution of the Riccati equation; $\alpha = -\pi/4$, $L = 7\,\text{cm}$.

viewpoint. On the other hand, this new approach can be beneficial in terms of two additional criteria, namely performance of the device (our examples have illustrated this point), and simplicity of numerical simulations. The next section will shed additional light on the last point.

4. Analysis in terms of spline functions

The previous section is quite far from exhausting all the cases of practical interest. Clearly, the maximum flexibility in filter design is achieved if the taper function $\gamma(z)$ is left arbitrary. To cover this case, we implemented a simple and efficient numerical algorithm. Our aim was to make simulations fast enough to be used in real time, during the grating manufacturing process. It is based on approximating the integrand in the right-hand side in (3) in terms of linear spline functions.

The first step consists of constructing a linear interpolation of profile samples. This produces a piecewise linear polynomial, say $P_1(z)$, continuous on the whole interval $[-L/2, L/2]$, nondifferentiable on the nodes, say $z_i, i=0, 1, 2, \ldots, n$. Then, all we need is to evaluate analytically the fFT of a linear function. If $y_i, i=0, 1, 2, \ldots, n$, are the sample values to be interpolated, we have

$$P_1(z)=\sum_{i=0}^{n}\phi_i(z)y_i, \tag{28}$$

$\phi_i(z)$ denoting suitable piecewise linear functions. Then, by the linearity of the fFT (Ozaktas *et al.* 2001),

$$\mathcal{F}^{\alpha}[P_1(A_1z)]=\mathcal{F}^{\alpha}\left[\sum_{i=0}^{n}\phi_i(A_1z)\,y_i\right]=\sum_{i=0}^{n}\mathcal{F}^{\alpha}[\phi_i(A_1z)]\,y_i, \tag{29}$$

hence, only the fFTs of the linear functions ϕ_i are needed. Defining the functions

$$\zeta_-(z)=\begin{cases}1+\frac{z}{L} & -L\le z<0,\\ 0 & \text{elsewhere,}\end{cases} \tag{30}$$

$$\zeta_+(z)=\begin{cases}1-\frac{z}{L}, & 0\le z\le L\\ 0 & \text{elsewhere,}\end{cases} \tag{31}$$

we have

$$\begin{aligned}&\phi_0(z)=\zeta_+(z-z_0), \quad \phi_n(z)=\zeta_-(z-z_n),\\ &\phi_i(z)=\zeta_-(z-z_i)+\zeta_+(z-z_i).\end{aligned} \tag{32}$$

Evaluating the fFTs of the ϕ's requires a little algebra that we omit for short. The result is

$$Z_-(x)\equiv\mathcal{F}^{\alpha}[\zeta_-(z)](x)=AB_-^1[\mathrm{erf}(x_0)-\mathrm{erf}(x_-)]+AB_-^2(e^{-x_0^2}-e^{-x_-^2}), \tag{33}$$

$$Z_+(x)\equiv\mathcal{F}^{\alpha}[\zeta_+(z)](x)=AB_+^1[\mathrm{erf}(x_+)-\mathrm{erf}(x_0)]+AB_+^2(e^{-x_+^2}-e^{-x_0^2}), \tag{34}$$

where A is defined in (22), and where we set

$$B_{\pm}^{1} = 1 \mp \frac{C_a}{B_a}\frac{x}{L}, \quad B_{-}^{2} = -\frac{1+j}{\pi L\sqrt{2B_a}}, \quad B_{+}^{2} = -B_{-}^{2},$$
$$x_0 = -(1-j)\sqrt{\frac{\pi}{2}}\frac{C_a}{\sqrt{B_a}}x$$
$$x_{\pm} = -(1-j)\sqrt{\frac{\pi}{2}}\left(\mp L\sqrt{B_a} + \frac{C_a}{\sqrt{B_a}}x\right). \tag{35}$$

Finally,

$$\mathcal{F}^{\alpha}[P_1(z)](x) = \sum_{i=0}^{n-1} Z_{+}(x-x_i)\, e^{\eta^{\alpha}(z_i)} y_i + \sum_{i=1}^{n} Z_{-}(x-x_i)\, e^{\eta^{\alpha}(z_i)} y_i, \tag{36}$$

where

$$x_i = z_i \cos\alpha, \qquad \eta^{\alpha}(z_i) = j\frac{\pi}{2}\nu - j2\pi\, x\, \bar{z}_i, \tag{37}$$

being

$$\nu = \bar{z}_i^2 \sin 2\alpha, \quad \bar{z}_i = z_i \sin\alpha. \tag{38}$$

Now we can evaluate the reflectivity for *any* given index profile, numerically, through the evaluation of known fFTs. Figure 12 shows the comparison between theoretical and numerically computed reflectivity, for raised cosine grating profiles. The latter has been obtained by the spline-function technique, for grating lengths $L = 1$ cm, 5 cm, and 7 cm. The number of samples was manually adapted to each of these lengths. Figure 13 refers to the same problem, and illustrates the dependence of the results on the number of samples, for a fixed grating length.

This approach can be incorporated into a real-time computer-aided manufacturing procedure. This statement is based on the fact that, very often, an FBG is written, physically, as a sequence of separate stretches. The spline function approach allows one to predict, quite simply, the reflectivity to be expected after writing each individual segment. If, after writing each piece, the reflectivity is measured and compared with predictions, information can be fed back, to affect the manufacturing of the remaining parts of the grating. A key issue, in this respect, is error propagation, to be discussed next.

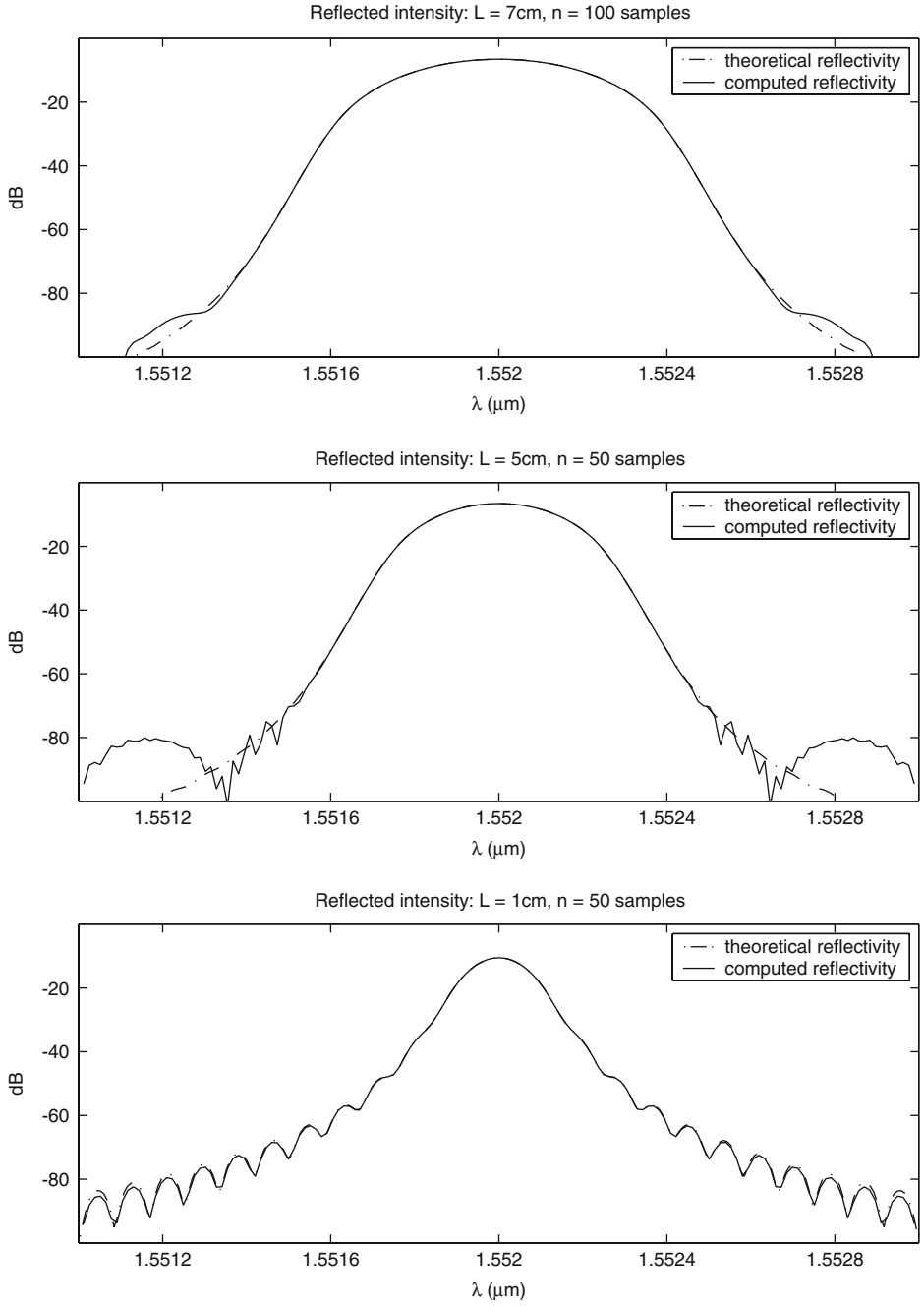

Fig. 12. Comparison between theoretical and numerically computed (by splines) reflectivity for gratings with a raised cosine profile, vs. wavelength; $L = 7\,\text{cm}$, $5\,\text{cm}$, $1\,\text{cm}$, but with an appropriate sample number.

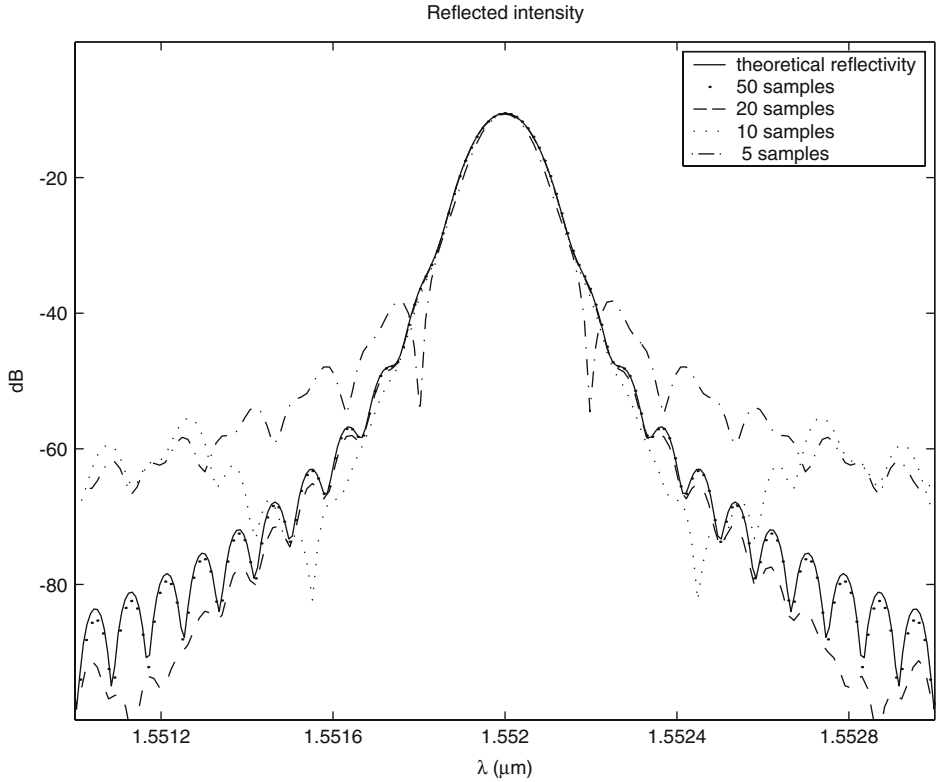

Fig. 13. Comparison between theoretical and numerically computed (by splines) reflectivity for a raised cosine grating, $L = 1$ cm, vs. wavelength, for several numbers of samples.

5. The effect of random errors

Experimentally, it is widely demonstrated that the performances of FBGs are strongly affected by random errors in their profile. To validate the design procedure based on f FT, we need to show that this technique is able to model errors. We shall follow the outline of (Feced and Zervas 2000). Let the actual index profile be

$$\Delta n(z) = A\gamma(z)\,[1 + F_a(z)] \cos\left(\frac{2\pi}{\Lambda} z + \phi(z)\right). \tag{39}$$

We assume that $F_a(z)$ is a gaussian, stationary, zero-mean process, with autocorrelation function given by

$$\langle F_a(z+\tau) F_a(z)\rangle = \eta\,\delta(\tau), \tag{40}$$

$\delta(\tau)$ being the Dirac delta function, essentially a white noise process. This means that the most important effects of the random perturbations described by the stochastic process $F_a(z)$ affect the amplitude but not the phase (the two are assumed to be uncorrelated). If the grating is sampled with a sufficiently small step size Δ, the variance for each sample can be expressed as

$$\sigma_a^2 = \frac{\eta}{\Delta}. \tag{41}$$

The quantity Δ^{-1} can be viewed as the upper cutoff spatial frequency of the broadband noise spectrum. Its value is determined, in practice, by the grating writing procedure, and is, in general, of the order of few hundreds of microns. The noise bandwidth is then large enough to validate the white noise assumption.

The coupling function

$$q(z) \equiv \kappa \gamma(z) e^{-j\phi(z)} \tag{42}$$

in the reflection coefficient integral (3) should be replaced now by

$$q(z) = \kappa \gamma(z)\,[1 + F_a(z)]\, e^{-j\phi(z)} \equiv q_0(z)\,[1 + F_a(z)], \tag{43}$$

where $q_0(z)$ denotes the corresponding function unaffected by random perturbations. The same relation as (3) connects $q(z)$ to the complex-valued reflection coefficient, which becomes, consequently, a stochastic process as well. We may then evaluate the expected value, say $\mathcal{R}(\xi)$, of the *reflectivity* $R(\xi) \equiv |r(\xi)|^2$,

$$\begin{aligned}\mathcal{R}(\xi) = \langle r(\xi) r^*(\xi) \rangle &= \left\langle \int_{-\frac{L}{2}}^{+\frac{L}{2}} dy \int_{-\infty}^{+\infty} \mathrm{d}x\, q(y) q^*(x)\, e^{-j2\xi(x-y)} \right\rangle \\ &= \left\langle \int_{-\frac{L}{2}}^{+\frac{L}{2}} dz \int_{-\infty}^{+\infty} d\tau\, q(z) q^*(z+\tau) e^{-j2\xi\tau} \right\rangle. \end{aligned} \tag{44}$$

Here we set $\tau = x - y, z = y$, and exploit the fact that $q(z)$ vanishes for $|z| > L/2$.

Things become clearer if we separate the deterministic part from the random one in (44), using (43). The reflectivity due to the deterministic part is

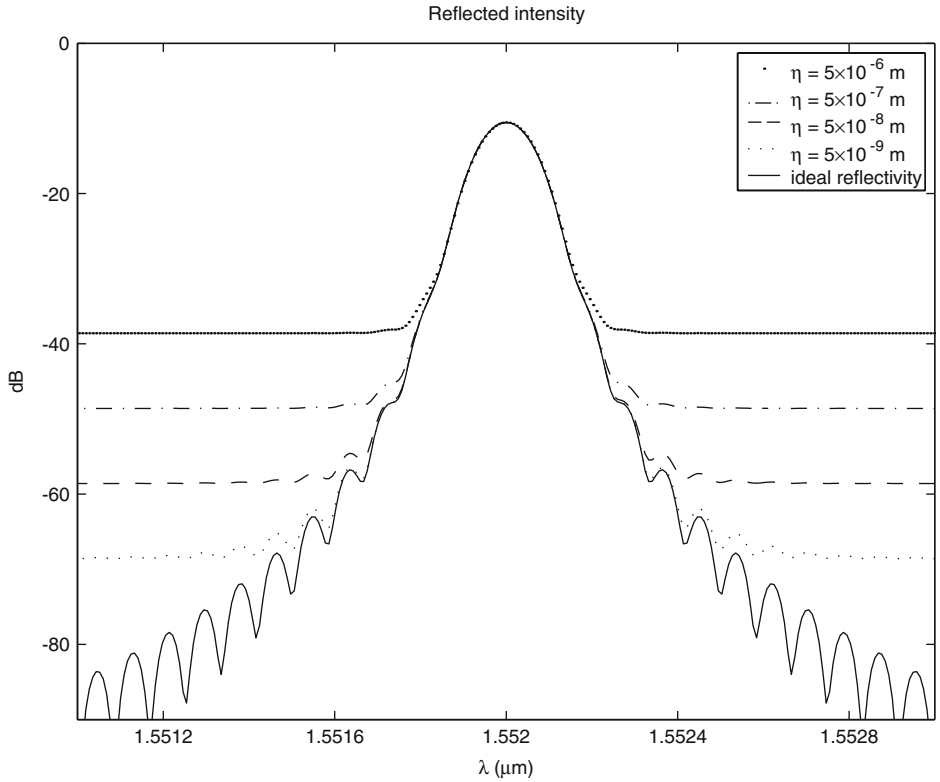

Fig. 14. Mean reflectivity for a raised cosine grating long $L = 1$ cm, affected by random writing errors. The parameter η sizes the error magnitude; the sampling step, $\Delta = 200$ μm, is constant.

the same as in previous sections, while the manufacturing errors are responsible for an error in reflectivity, expressed by

$$\begin{aligned}\mathcal{R}_{\text{error}}(\xi) &= \int_{-\frac{L}{2}}^{+\frac{L}{2}} \mathrm{d}z \int_{-\infty}^{+\infty} \mathrm{d}\tau\, q_0(z) q_0^*(z+\tau)\, e^{-j2\xi\tau}\, \langle F_a(z+\tau) F_a(z)\rangle \\ &= \int_{-\frac{L}{2}}^{+\frac{L}{2}} \mathrm{d}z \int_{-\infty}^{+\infty} \mathrm{d}\tau\, q_0(z) q_0^*(z+\tau)\, e^{-j2\xi\tau}\, \eta\, \delta(\tau) \\ &= \int_{-\frac{L}{2}}^{+\frac{L}{2}} \mathrm{d}z\, \eta\, |q_0(z)|^2 = \eta\kappa^2 \int_{-\frac{L}{2}}^{+\frac{L}{2}} \mathrm{d}z\, \gamma^2(z). \end{aligned} \tag{45}$$

Here (40) has been used, besides the properties of the delta functions. Finally, we get

$$\mathcal{R}(\xi) = R(\xi) + \mathcal{R}_{\text{error}}(\xi) = |r(\xi)|^2 + \eta\kappa^2 \int_{-\frac{L}{2}}^{+\frac{L}{2}} \mathrm{d}z\, \gamma^2(z). \tag{46}$$

As an example, for a raised cosine profile we obtain

$$\mathcal{R}(\xi) = |r(\xi)|^2 + \eta\kappa^2 \int_{-\frac{L}{2}}^{+\frac{L}{2}} \mathrm{d}z \, \frac{1}{2}\left[1 + \cos\left(\frac{2\pi z}{L}\right)\right] = |r(\xi)|^2 + \frac{3}{4}\eta\kappa^2 L. \qquad (47)$$

At this point, we take the opportunity to exploit the efficient evaluation of the unperturbed reflectivity, $|r(\xi)|^2$, offered by the f FT, as shown above.

As typical numerical values, we take $L = 1$ cm, $\lambda_B = 1.552\mu$m, $A = 3 \times 10^{-5}$, and a sampling step size $\Delta = 200\mu$m. In Fig. 14, the mean reflectivity is plotted as a function of η, i.e. of the size of the manufacturing errors. It shows that such errors cause a background 'plateau': the reflectivity outside the filter stop-band is higher than for a perfect device, and does not decrease as the wavelength gets farther from the peak. The dynamic range is then significantly reduced. Note that, in our examples, the FBG length, L, has been chosen rather short, to emphasize this feature.

To validate the formula (47), we have compared the results shown in Fig. 15 with Monte Carlo simulations, made as follows. The reflectivity integral in (3), for an index profile perturbed according to (39), was evaluated numerically for different realizations of the noise. Next, a suitable average was made. For the purpose of illustration, Figure 15 shows the results for four independent realizations, corresponding to four different values of η, with a sample step size $\Delta = 200\,\mu$m. The mean reflectivity spectra agree very well with those shown in Fig. 15, obtained using the f FT approach.

6. Grating synthesis

The possibility of expressing the reflection coefficient (3) as an f FT entails another significant advantage. The f FT can be inverted, similarly to the ordinary FT, and the inverse transformation can also be expressed as a fractional FT. Hence, it is possible to express the index profile, $\gamma(z)$, in terms of a transform of the reflection coefficient, $r(\xi)$. This is an attractive, potentially cheap way to solve the *synthesis* problem: from a given complex-valued reflection coefficient to the corresponding index profile. In principle, the same goal is achievable by means of a numerical quadrature. However, let us stress that, in general, such an 'inverse problem' should be expected to be much harder to solve than the (semi-)analytical evaluation of the inverse f FT.

Let us suppose that a suitable number of samples of a given reflection coefficient vs. wavelength are available. If we stick to the assumptions and

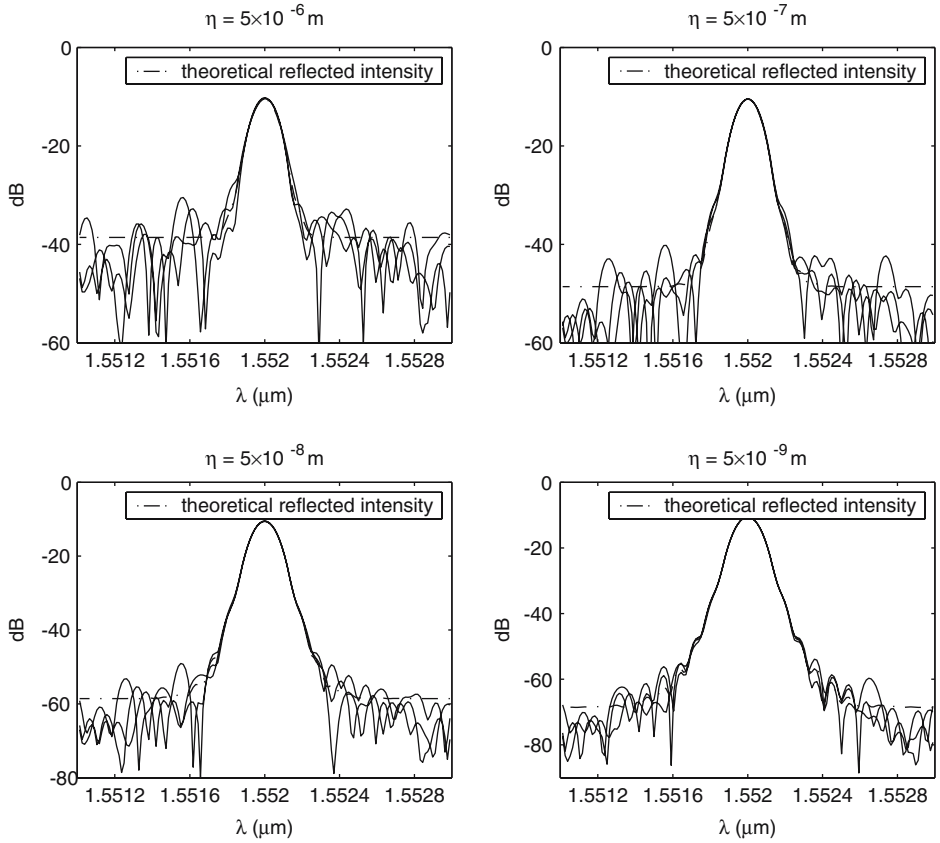

Fig. 15. Four realizations obtained by the analysis algorithm (correspondingly to four values of η), for a raised cosine grating, affected by writing errors, are compared with the mean theoretical reflectivity.

the symbols of the previous sections, these data are samples of a function of the type

$$r(\xi) = \beta_\alpha \, e^{-j\pi \, (\cot \alpha) \, (\xi / A_2)^2} \mathcal{F}^\alpha \left[\gamma \, (A_1 z) \right] \left(\frac{\xi}{A_2} \right), \tag{48}$$

where we set

$$\beta_\alpha = -\kappa \, \frac{\Lambda}{\sqrt{2C'}} \sqrt{\cos \alpha} \, e^{-j \frac{\pi}{4}} \, e^{-j \frac{\alpha}{2}} \tag{49}$$

(compare with (12)). Parameters to be chosen are the fractional order α of the fFT, and the number of samples to be used. All the other parameters, which enter (48) through the quantity β_α, can be considered as given.

Equation (48) can be inverted to yield

$$\gamma(A_1 z) = \frac{1}{\beta_\alpha}\, \mathcal{F}^{-\alpha}\left[r(\xi)\, e^{j\pi(\cot\alpha)\,(\xi/A_2)^2}\right](z), \tag{50}$$

where $\mathcal{F}^{-\alpha}$ denotes the *inverse* f FT of order α. To simplify the notation, define

$$\sigma = \frac{\xi}{A_2}, \qquad s(z) = \gamma(A_1 z),$$
$$S_a(\sigma) = \frac{1}{\beta_\alpha}\, e^{j\pi(\cot\alpha)\sigma^2} r(A_2\sigma). \tag{51}$$

The scaled profile $s(z)$ is defined on the interval $[-L/(2A_1), L/(2A_1)]$, while the domain of $S_a(\sigma)$, in general, is the entire real axis. Hence, in principle, an infinite series is required to compute the inverse f FT. However, it is easy to see that the f FTs of all the profiles that we considered in this paper, including the spline functions, are appreciably different from zero only on a bounded interval, centered on the Bragg wavelength. It can be shown in more detail that all the f FTs essentially vanish for $|\sigma| > 5$, cf. (Mazzetto 2003). Therefore, each f FT we use is defined on a bounded interval; hence, the number of the required samples is finite.

The main steps of our synthesis algorithm are the following:

- estimate the f FT's support;
- evaluate the maximum sampling period, F_{sup}, of the f FT;
- introduce a suitable set of samples of the reflection coefficient;
- evaluate $S_a(\sigma)$;
- evaluate the inverse transform of $S_a(\sigma)$, to obtain

$$s(t) = \overline{K}_a\, e^{-j\pi B_a t^2} \sum_{k\in\mathbf{Z}} F\, S_a(kF)\, e^{-j\pi B_a (kF)^2}\, e^{j2\pi C_a kFt}; \tag{52}$$

- change scale (according to the factor A_1) to obtain $\gamma(z)$.

We need to choose the sampling frequency, F. To avoid aliasing errors, this F should be chosen in such a way to make the a-periodicization period $T_p = 1/F|C_a|$ larger than the length T_s of the interval where $s(z) \neq 0$. If F_{sup} denotes the maximum period with which its transform can be sampled, then, according to the sampling theorem,

$$F < F_{\text{sup}} = \frac{1}{T_s|C_a|}. \tag{53}$$

A few examples will illustrate the algorithm, and test its reliability. For the ease of comparison, they will refer to gratings of the types described

in previous sections. Each example proceeds as follows. We start from the analytical expression of a given profile, and compute a sampled version of its f FT. From these samples, we compute the inverse f FT, and then compare the results with the original profile. All gratings are located on an interval of length $2D'$, hence we take $T_s = 1.2(2D')$. Recall that $\sigma = \xi/A_2 = -(\pi/A_2\Lambda)(\Delta\lambda)/\lambda$, thus

$$\lambda = \frac{\lambda_B}{1 + \frac{A_2 \Lambda \sigma}{\pi}}. \tag{54}$$

B_σ denotes the bandwidth in terms of the coordinate σ.

6.1. UNIFORM GRATING

Let $L = 7$ cm be the length of a uniform grating. It is reasonable to approximate its f FT assuming that it vanishes for $|\sigma| > 5$, cf. (Mazzetto 2003), thus obtaining a band-limited signal $s(z)$ with $B_\sigma = 5$. We also find $T_s = 10.86$, $F_{\text{sup}} = 0.065$. Hence, the minimum number of equally spaced samples to be used is $N_c = 2B_\sigma/F_{\text{sup}} = 154$. The values of λ corresponding to the endpoints $\sigma = \pm 5$ are $\lambda_{\min} = 1.55124$ μm, $\lambda_{\max} = 1.55276$ μm. From these data we recover, via the inverse f FT, the index profile, compared with the original one in Fig. 16. The synthesis error (i.e., the percent difference between the two profiles), is displayed in the lower part of the same Figure. The absolute value of the inverse f FT is plotted, rather than its real part (which would yield the original rect function), to show that aliasing errors do not affect the procedure. The synthesis error has been computed as the difference between the real part of the f FT and the function $\gamma(z)$ in $[-L/2, L/2]$. On such interval, the imaginary part of the f FT is nearly zero, its smallness resulting from the approximation made for the support of f FT. The synthesis error is less than 4%, the maximum values being at the endpoints of the grating. The ripples observed in this figure should be expected, since the same phenomenon occurs also for ordinary FTs, and is due to the discontinuity of the rect profile at the endpoints $\pm L/2$. Such an error can be reduced increasing the bandwidth. For $B_\sigma = 10$, a maximum error of less than 1% was recorded. In the central part of the interval such an error is actually very close to 0.2%. Outside that interval, both the real and the imaginary parts of the inverse f FT turn out not to be zero, and are modulated by a complex exponential. This, however, remains a matter of curiosity, and does not affect the usefulness of the synthesis procedure.

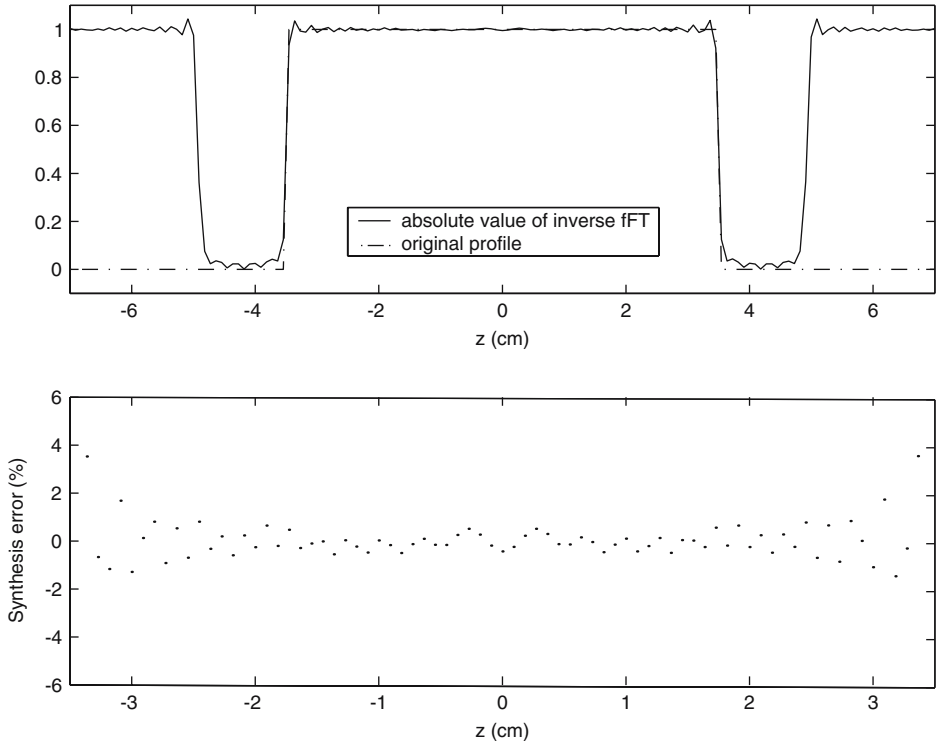

Fig. 16. Upper part: comparison between the inverse fractional Fourier transform and the original profile. Lower part: synthesis error for a grating with a constant index step, long $L = 7$ cm.

6.2. RAISED COSINE PROFILE

We take again $L = 7$ cm and $B_\sigma = 5$, and repeat the same procedure. The synthesis error is now less than about 10^{-5}, so that the bandwidth can be reduced to $B_\sigma = 3$, thus reducing the number of required equally spaced samples to $N_c = 93$ in the interval between $\lambda_{\min} = 1.55154$ μm and $\lambda_{\max} = 1.55246$ μm. The main results for this and the following examples are summarized in Table 1.

Table 1. Maximum synthesis error for various profiles and bandwidth

Bandwidth		Maximum synthesis error			
B_σ	Spectrum	Constant index step	Hyperbolic tangent	Raised cosine	Gaussian
3	0.9 nm	inadeq.	inadeq.	0.5%	0.01%
4	1.2 nm	inadeq.	0.5%	–	–
5	1.5 nm	4%	0.15%	0.003%	0.001 %
10	3 nm	1%	–	–	–

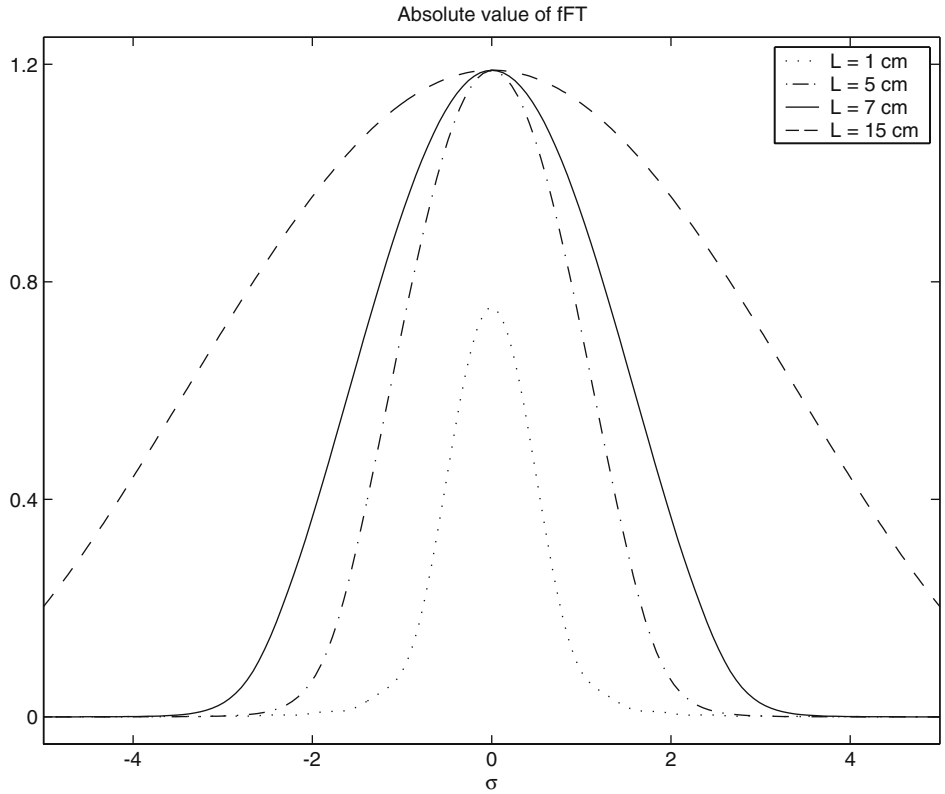

Fig. 17. Fractional Fourier transform of raised cosine profiles, for several gratings lengths.

6.3. GAUSSIAN PROFILE

Performances are very similar to those of the raised cosine profile, both profiles being essentially nonzero, within a high accuracy, on a bounded interval. In this case, the key parameter is the function width at half maximum, W, that we choose equal to 2 cm. The values $B_\sigma = 3$ and $B_\sigma = 5$ have also been used. The number of needed samples is rather small. Results for this case look even better than the previous ones, due to the higher selectivity of the gaussian profile (see Fig. 6).

6.4. HYPERBOLIC TANGENT PROFILE

Let us choose $T = 3.5$ in (23). The f FT of such a profile has been seen to be appreciably different from zero on an interval which is longer than in the previous cases (2) and (3), but still well bounded within the band-

Table 2. Maximum synthesis error for a raised cosine grating, for various grating lengths and bandwidth.

Maximum synthesis error					
B_σ	Device length				
	1 cm	5 cm	7 cm	10 cm	15 cm
5	0.1%	0.005%	0.003 %	0.04%	3%
10	0.02%	0.0002%	0.0001%	0.0001%	0.0004%

width $B_\sigma = 4$. Thus, we need just $N_c = 123$ samples, in the interval between $\lambda_{\min} = 1.55139$ μm and $\lambda_{\max} = 1.55261$ μm. The results corresponding to $B_\sigma = 4$ and $B_\sigma = 5$ were also evaluated, see Table 1.

In all cases, we noticed that the dependence of the synthesis results on the device length, L, is rather critical. From Fig. 17 we understand why shorter gratings, exhibiting a more localized profile, apparently lend themselves to a more accurate synthesis. However, shorter gratings are also characterized by lower central peaks. Hence, the lateral tails are, comparatively, less negligible. As a rule of thumb, we may say that our algorithm works well, in practice, for lengths of, say, $L = 5 \div 10$ cm, while precision in computation can be improved by choosing wider bands, see Table 2.

The main results concerning our synthesis algorithm are summarized in Table 1. The maximum numerical errors are given for grating various profiles and values of the bandwidth B_σ.

7. Conclusions

We have shown that the so-called fractional Fourier Transform (f FT) can be conveniently applied to the analysis and synthesis process of fiber Bragg gratings. A number of refractive index profiles, for which the f FT is known analytically, have been chosen, to illustrate how the procedure works. The f FT, while generalizing the ordinary FT, retains most of its properties, and many of them can be exploited to speed up calculations. The very important issue of accuracy has been addressed by comparing f FT-based results with those obtained by numerical integration of the full Riccati equation, to which f FT stays as a Born approximation. It has been found that the agreement remains surprisingly good even for relatively high reflectivities: spectral shapes are always reproduced very faithfully, while, in the worst cases, peak reflectivities are only slightly over-estimated by the f FT.

In the case of FBG analysis, one of the main tasks is to study how, given the shape of the index profile, the parameters affect the FBG response. Then, an important advantage of this new procedure is that, for most of the 'classical' profiles, the f FT is known analytically. In all these cases, the processing time required for subsequent numerical evaluation is propor-

tional to the number of samples that describe the grating profile. In the numerous runs that we made, dealing with all the aforementioned profiles, the processing times were, at most, fractions of a second on a PC. Hence, they seem to be compatible with *real-time* operations, made while a grating is being manufactured.

One of the most important properties of the fFT is that the inverse transformation is known, and very similar to the direct one. This makes the procedure suitable for synthesizing the FBG index profile, once its (complex) reflection coefficient is given. The properties and performances of the synthesis algorithm have been discussed in detail. They look attractive enough to conclude that this algorithm could become part of a computer-aided FBG manufacturing process. The method we followed in this paper is, in principle, limited by the assumption of low reflectivity. In fact, in the Riccati equation, rigorously satisfied by the reflection coefficient, there is a quadratic term, which was neglected to obtain the expression the fFT starts from. However, several comparisons that we made with numerical solutions of the Riccati equation show that, for devices of practical interest, discrepancies are quite low, for both the amplitude and the group delay of the reflection coefficient. At the same time, the CPU time required by the fFT approach is at least 3 orders of magnitude smaller than by the Runge-Kutta integration of the Riccati equation.

Acknowledgements

This work was supported, in part, by the Italian GNFM–INdAM; R. S. was with DEI, University of Padova, on leave from the University of "Roma Tre".

References

Abramowitz, M. and I.A. Stegun, *Handbook of Mathematical Functions*. Dover, New York, 1970.

Azana, J. and M.A. Muriel, *IEEE J. Select. Topics Quantum Electron.* **7** 728, 2001.

Baghdasaryan, H.V., G.G. Karapetyan, S.I. Avagyan, T.M. Knyazyan, and G.M. Haroutounyan. In: *43rd Int. Sci. Colloq.*, Technical Univ. Illmenau, September 21–24, 1998.

Bonino, S., M. Norgia and E. Riccardi, *11th Int. Conf. on Integrated Optics and Optical Fibre Communications, 23rd European Conf. on Optical Comm.*, IOOC–ECOC 97 Conf., Publ. No. 448, Vol. 3. 194, 1997.

Braghetto, S. Applicazione della Trasformata di Fourier Frazionaria ai Reticoli di Bragg, "Laurea" Thesis, University of Padua, 1998 (in Italian).

Erdogan, T. *IEEE J. Lightwave Techn.* **15** 1277, 1997.

Erseghe, T. Trasformata di Fourier frazionaria, "Laurea" Thesis, University of Padua, 1996 (in Italian).

Feced, R., M.N. Zervas, and A. Muriel, *IEEE J. Quantum Electron.* **35**, 1105, 1999 .
Feced, R.C. and M.N. Zervas, *IEEE J. Lightwave Techn.* **18**, 90, 2000.
Galli, P. Teoria dei Reticoli di Bragg in Termini di Trasformata di Fourier Frazionaria, "Laurea" Thesis, University of Padua, 1999 (in Italian).
Kashyap, R. *Fiber Bragg Gratings,* 1st edn. Academic Press, San Diego, 1999.
Keren, S., A. Rosenthal and M. Horowitz, *IEEE Photon. Technol. Lett.* **15**, 575, 2003.
Kogelnik, H. *Bell System Tech. J.* **55**, 109, 1976.
Mazzetto, E. Applicazione della trasformata di Fourier frazionaria ad analisi e sintesi di filtri a reticoli di Bragg, "Laurea" Thesis, University of Padua, 2003 (in Italian).
McBryde A.C. and F.H. Kerr, *IMA J. Appl. Math.* **39**, 159, 1987.
McCall, M. *IEEE J. Lightwave Techn*. **18**, 236, 2000.
Namias, V. *IMA J. Appl. Math.* **25**, 241, 1980.
Ouellette, F., J.-F. Cliche and S. Gagnon, *IEEE J. Lightwave Techn.* **12**, 1728, 1994.
Ouellette, F., P.A. Krug, T. Stephens, G. Dhosi and B. Eggleton, *Electron. Lett.* **31**, 899, 1995.
Ozaktas, H.M., Z. Zalevsky and M.A. Kutay, *The Fractional Fourier Transform (with Applications to Optics and Signal Processing)*. Wiley, Chichester, 2001.
Pellat-Finet, P. *Opt. Lett.* **19**, 2622, 1994.
Schiavone, L. Analisi e Sintesi di Reticoli di Bragg Mediante la Trasformata di Fourier Frazionaria, "Laurea" Thesis, University of Padua, 2000 (in Italian).
Skaar, J., L. Wang and T. Erdogan, *IEEE J. Quantum Electron.* **37**, 165, 2001.
Song, G.-H. and S.-Y., Shin. *J. Opt. Soc. Am. A*, **2**, 1905, 1985.
Yariv, A. *IEEE J. Quantum Electronics* **QE-9** 919, 1973.
Wang, L. and T. Erdogan, *Electron. Lett.* **37**, 154, 2001.
Weller-Brophy, L.A. and D.G. Hall, *J. Opt. Soc. Amer.* **A-2** 863, 1985.
Weller-Brophy, L.A. and D.G. Hall, *J. Opt. Soc. Amer.* **A-4** 60, 1985.
Weller-Brophy, L.A. and D.G. Hall, *Appl. Opt.* **27** 963, 1988.